ANNUAL REVIEWS

Annual Review of Physical Chemistry

Electrochemical Tip-Enhanced Raman Spectroscopy: An In Situ Nanospectroscopy for Electrochemistry

Sheng-Chao Huang, Yi-Fan Bao, Si-Si Wu, Teng-Xiang Huang, Matthew M. Sartin, Xiang Wang, and Bin Ren

State Key Laboratory of Physical Chemistry of Solid Surfaces, Collaborative Innovation Center of Chemistry for Energy Materials (iChEM), College of Chemistry and Chemical Engineering, Xiamen University, Xiamen 361005, China; email: wangxiang@xmu.edu.cn, bren@xmu.edu.cn

Annu. Rev. Phys. Chem. 2021. 72:213–34

First published as a Review in Advance on January 5, 2021

The *Annual Review of Physical Chemistry* is online at physchem.annualreviews.org

https://doi.org/10.1146/annurev-physchem-061020-053442

Keywords

electrochemistry, tip-enhanced Raman spectroscopy, nanospectroscopy, scanning probe microscopy, vibrational spectroscopy, spatial resolution

Abstract

Revealing the intrinsic relationships between the structure, properties, and performance of the electrochemical interface is a long-term goal in the electrochemistry and surface science communities because it could facilitate the rational design of electrochemical devices. Achieving this goal requires in situ characterization techniques that provide rich chemical information and high spatial resolution. Electrochemical tip-enhanced Raman spectroscopy (EC-TERS), which provides molecular fingerprint information with nanometer-scale spatial resolution, is a promising technique for achieving this goal. Since the first demonstration of this technique in 2015, EC-TERS has been developed for characterizing various electrochemical processes at the nanoscale and molecular level. Here, we review the development of EC-TERS over the past 5 years. We discuss progress in addressing the technical challenges, including optimizing the EC-TERS setup and solving tip-related issues, and provide experimental guidelines. We also survey the important applications of EC-TERS for probing molecular protonation, molecular adsorption, electrochemical reactions, and photoelectrochemical reactions. Finally, we discuss the opportunities and challenges in the future development of this young technique.

1. INTRODUCTION

Electrochemistry is receiving increasing attention, especially recently, due to its broad application in such various areas as batteries, fuel cells, corrosion, synthesis, and catalysis as well as its important role in our daily lives. In an electrochemical system, various complex processes, including adsorption, desorption, and diffusion of species; surface reconstruction; charge transfer between the surface and species; the formation or breaking of chemical bonds; and chemical reactions, take place at the electrochemical interface. Therefore, the structure of the electrochemical interface determines the electrochemical response and the properties and performance of the whole electrochemical system. There is a long-term effort to reveal the intrinsic relationships between structure, property, and performance to promote the design of materials for electrochemical devices.

Conventional electrochemical characterization techniques, which are based on the measurement of electrical signals, including current and potential, are the most basic and widely used methods for understanding an electrochemical system. A wealth of information, including thermodynamic and kinetic information about interfacial properties, the amount of reacting species on the surface, and the reactivity of the electrodes, can be obtained by analyzing the electrical signals according to electrochemical theory (1). However, the lack of chemical fingerprint information on the reacting species makes it challenging to identify the chemical structure without prior knowledge of the species. Additionally, the measured electrical signal comes from the response of the whole electrode surface, making it a challenge to spatially resolve the heterogeneity of the structure and properties on an inhomogeneous electrode surface (**Figure 1*a***). Conventional electrochemical methods have reached their limit in meeting the growing requirements of characterizing complex and sophisticated electrochemical systems, which are usually dynamic in time and space in the nanoscale dimension. Therefore, it is desirable to develop in situ characterization methods with rich chemical information and high spatial resolution, up to several nanometers, for a comprehensive understanding of electrochemical interfaces and processes.

A convenient way to obtain in situ chemical information is to employ spectroscopic techniques such as electronic spectroscopy [ultraviolet-visible (UV-Vis) absorption (2) and fluorescence spectroscopy (3)], vibrational spectroscopy [infrared (IR) (4), Raman (5), and sum-frequency generation (SFG) spectroscopy (6)], and X-ray spectroscopy [X-ray absorption spectroscopy (XAS) (7)/X-ray absorption fine-structure spectroscopy (XAFS) (8), X-ray diffraction (XRD) spectroscopy (9), and other X-ray scattering spectroscopies (10)], which have been combined with electrochemistry to result in a field called spectroelectrochemistry (**Figure 1*a***). Among these techniques, vibrational spectroscopy can provide molecular fingerprint information without the requirement for an expensive synchrotron light source. Among various vibrational spectroscopic methods, Raman spectroscopy is particularly powerful for characterizing the electrochemical interface for the following reasons: It can work in the presence of electrolyte solutions because the Raman scattering intensity of water is weak and the interference is low; visible laser light can be used as the excitation source; and the full energy range of vibrational modes of chemical species can be detected.

Raman scattering is an inelastic scattering process. When a molecule is excited by the light, the electron cloud of the molecule is deformed and polarized to absorb photons, generating a virtual state with a higher energy. With very low probability, the polarized electron cloud can exchange energy with the vibration of nuclei via vibronic-electronic coupling, scattering photons with an energy that is different from incident photons. This is Raman scattering, and the energy difference, reflecting the vibration of nuclei, is termed the Raman shift. The Raman shift and the relative intensities of vibrational modes can reflect the bond strength and the atoms contributing to the modes and the surrounding chemical environment (11, 12). As a result, Raman spectroscopy

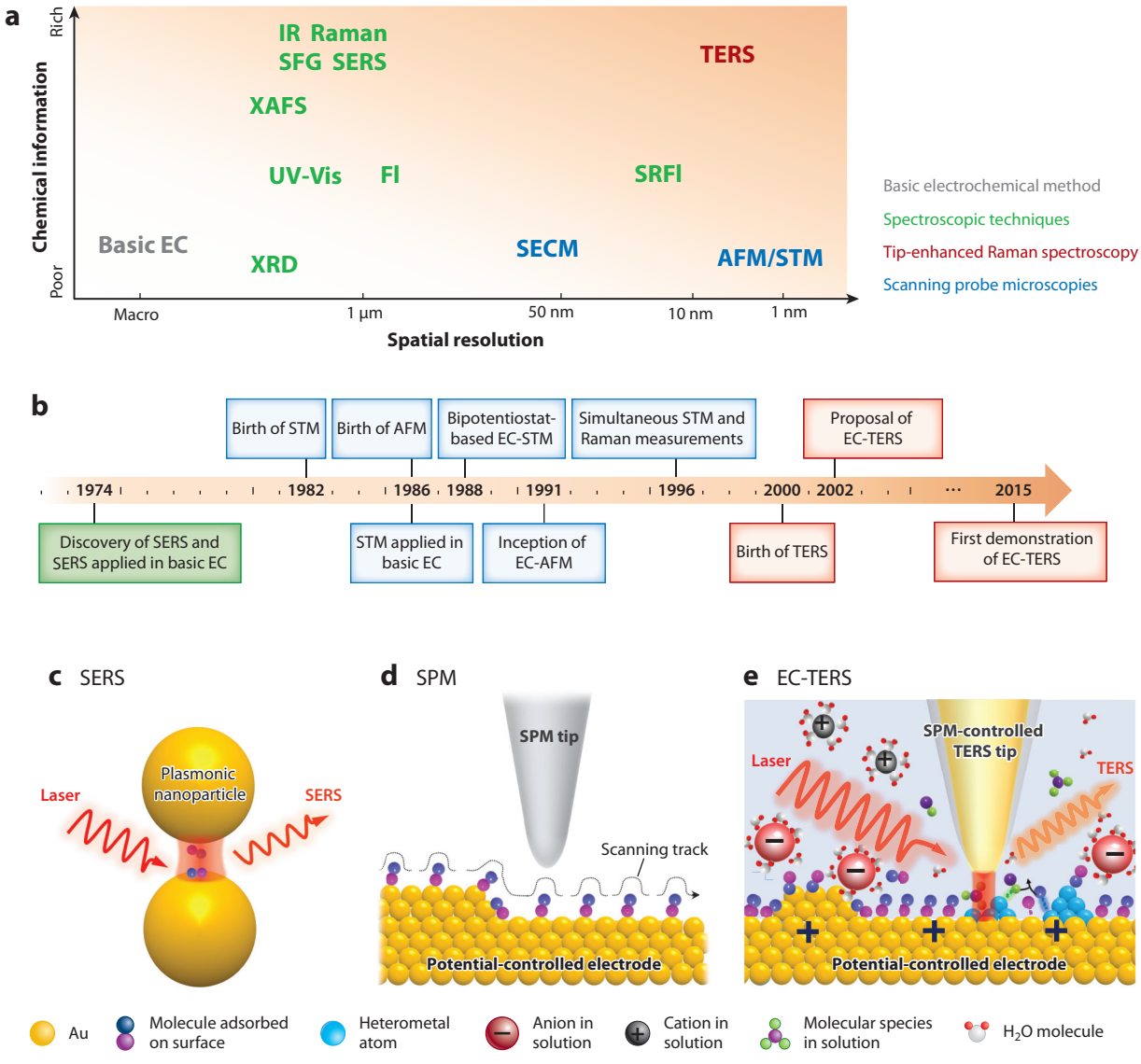

Figure 1

(*a*) Graph showing in situ characterization techniques for investigating electrochemical systems. (*b*) Timeline of milestone techniques leading to the development of EC-TERS. (*c–e*) Schematic illustrations of SERS, SPM, and EC-TERS, respectively. Abbreviations: AFM, atomic force microscopy; basic EC, basic electrochemical method; EC-AFM, electrochemical atomic force microscopy; EC-STM, electrochemical scanning tunneling microscopy; EC-TERS, electrochemical tip-enhanced Raman spectroscopy; Fl, fluorescence spectroscopy; IR, infrared spectroscopy; Raman, Raman spectroscopy; SECM, scanning electrochemical microscopy; SERS, surface-enhanced Raman spectroscopy; SFG, sum-frequency generation; SPM, scanning probe microscopy; SRFl, super-resolution fluorescence spectroscopy; STM, scanning tunneling microscopy; TERS, tip-enhanced Raman spectroscopy; UV-Vis, ultraviolet-visible absorption spectroscopy; XAFS, X-ray absorption fine-structure spectroscopy; XRD, X-ray diffraction spectroscopy.

is widely used to determine molecular structures and their interactions with the environment. In addition, Raman intensity is proportional to the number of molecules, so it can be used for quantitative analysis. However, due to the inherently weak inelastic scattering efficiency of the Raman process, only about one in every 10^6–10^{10} incident photons is Raman scattered, making it difficult to directly probe monolayer species at the electrochemical interface.

However, the discovery of surface-enhanced Raman spectroscopy (SERS) in the 1970s (5, 13, 14) greatly expanded the application of Raman spectroscopy for electrochemistry (**Figure 1*b***). The SERS effect is boosted by the localized surface plasmon resonance (LSPR) effect of noble metal nanostructures (**Figure 1*c***). The LSPR is the collective oscillation of free electrons in the noble metal nanostructure excited by light of a suitable wavelength, which can tightly confine and strongly enhance the electromagnetic field surrounding the metal nanostructure surface (15–17). As a result, the Raman intensity of molecules on the metal surface can be amplified by over a million times, making SERS a suitable tool for the in situ probing of electrochemical interfaces and interfacial processes with submonolayer and even single-molecule sensitivity (18, 19). However, the requirement for the noble metal nanostructure in SERS restricts its general application to a limited number of electrode surfaces. This shortcoming can be partially overcome by using shell-isolated nanoparticle-enhanced Raman spectroscopy (SHINERS). By depositing Au or Ag nanoparticles coated with an ultrathin inert shell onto the electrode surface and borrowing the enhancement from the Au or Ag core, SHINERS can be applied to various electrode surfaces that do not support a large surface-enhancement effect and to single-crystal surfaces that do not show a SERS effect (20–24). The ultrathin inert shell can minimize the chemical and electronic interference of nanoparticles with the probed electrode surface. Both SERS and SHINERS are far-field techniques performed using a conventional optical microscope; hence, the spatial resolution is limited by optical diffraction to the submicrometer level, which does not meet the requirement for nanoscale chemical imaging of electrochemical interfaces.

The development of scanning probe microscopy (SPM) offers a way to characterize the electrode surface with nanoscale or atomic spatial resolution (**Figure 1*a***). Electrochemical scanning tunneling microscopy (EC-STM) and electrochemical atomic force microscopy (EC-AFM), implemented in the 1980s (25–27) and 1990s (28) (**Figure 1*b***), respectively, can provide in situ topographic information on the electrode surface (**Figure 1*d***), which allows determination of the atomic structure of the electrode surface, the configurations of adsorbed species, and the structures of specific active sites during electrochemical deposition. Scanning electrochemical microscopy (SECM), which involves measurement of the current through an ultramicroelectrode when it is held or moved over an electrode (substrate) surface, provides information about local electrochemical properties and the reactivity of the substrate at micro- or nanoscale resolution (29–32). These electrochemical SPM (or EC-SPM) techniques provide high spatial resolution that is not possible using conventional electrochemical methods. However, SPM cannot provide chemical fingerprint information.

To simultaneously obtain topographic and molecular fingerprint information for the electrode surface, Tian et al. (33) combined STM with a fiber-based Raman spectrometer in 1996. In this case, the Raman signal was from the electrode surface illuminated by the laser; therefore, the spatial resolution of the Raman measurement was still diffraction limited. This problem can be overcome by tip-enhanced Raman spectroscopy (TERS) (**Figure 1*a***). TERS combines plasmon-enhanced Raman spectroscopy and SPM techniques (34–37) by replacing the W or Pt–Ir tip with a plasmonic Au or Ag tip. Under the illumination of a laser with the proper wavelength and polarization, the nanometer-sized Au or Ag tip apex with a strong LSPR effect can confine the electromagnetic field and enhance the Raman scattering of the sample species close to the tip apex, offering single-molecule sensitivity and nanometer (and even subnanometer) spatial resolution. These

benefits, together with its ability to work in aqueous solution, make TERS a promising tool for molecular-level and nanoscale analysis of electrochemical interfaces and processes (**Figure 1*e***).

We proposed the idea of combining TERS with electrochemistry as early as 2003 (38), just two years after the discovery of TERS. However, due to technical challenges, the first electrochemical TERS (EC-TERS) work was not reported until 2015 (**Figure 1*b***) (39, 40). It is now timely to review and summarize the development of EC-TERS over the past 5 years and to discuss the future development of this young but promising technique. In this review, we first discuss the challenges encountered when extending TERS from the ambient environment to the electrochemical environment and introduce the development of EC-TERS setups. Then, we discuss tip-related issues in EC-TERS and provide experimental guidelines, followed by coverage of current progress in the application of EC-TERS to the study of electrochemical interfaces and processes, including molecular protonation, molecular adsorption, electrochemical reactions, and photoelectrochemical reactions. Finally, we discuss the opportunities and challenges in the future development of the EC-TERS technique for a wide variety of applications in electrochemistry.

2. IMPLEMENTATION OF EC-TERS

EC-TERS involves a complex combination of a potentiostat, SPM (sensitive to vibrational interference with limited open space), and a Raman microscope. Although prior technical knowledge on the EC-SERS and electrochemical SPM techniques provides some support to the development of EC-TERS, extending TERS from air to the electrochemical environment is still very challenging. In comparison with the 5 years' time used to develop EC-STM (or EC-AFM) from STM (or AFM), it took a much longer time (about 15 years) to successfully push TERS to the electrochemical environment (**Figure 1*b***). The technical challenges lie mainly in the EC-TERS setup and tip-related issues in practical experiments.

2.1. EC-TERS Setups

When developing an EC-TERS setup, the first challenges to be overcome are those relating to the extension of TERS to the liquid environment. When light passes from air to the electrolyte solution, the optical path is severely distorted as a result of the mismatched refractive indices. The optical distortion dramatically reduces the image quality of the view of the tip apex and leads to defocusing of the laser spot, making it very challenging to achieve precise optical coupling and high-efficiency excitation of the single plasmonic hot spot beneath the tip. Therefore, the Raman optical path should be optimized to minimize the optical distortion in the EC-TERS system. There is a conflict between the limited space of the commercial EC-SPM with its compact structure and the requirement for adequate open space to accommodate the high numerical aperture (NA) optics needed to achieve high excitation and collection efficiency. Thus, both the Raman optical system and the EC-SPM system should be carefully designed and optimized to accommodate each other to maintain the high performance of the EC-SPM and achieve the necessary high efficiency of the Raman optical system.

Three optical configurations commonly used in ambient conditions can be modified for the electrochemical environment (**Figure 2*a*,*d*,*f***). In the side-illumination configuration, the light passes through a meniscus liquid layer formed due to the capillary force of the tip, which severely distorts the optical path (**Figure 2*a***). To reduce the optical distortion, we developed the first EC-TERS setup based on a modified side-illumination configuration (**Figure 2*b***) (39). In this setup, the laser beam was introduced into the specially designed electrochemical cell horizontally and focused via an objective onto the tip apex. The substrate was tilted 10° to decrease the amount

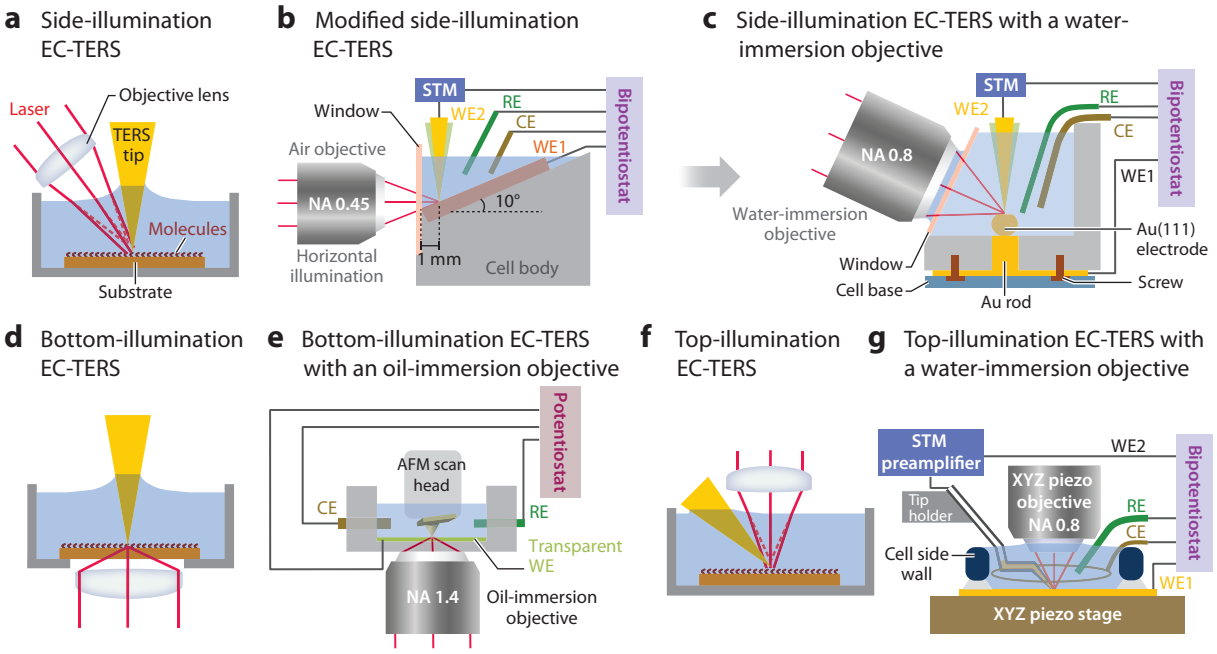

Figure 2

(*a*,*d*,*f*) Schematic illustrations of side-illumination, bottom-illumination, and top-illumination optical configurations, respectively, for EC-TERS. (*b*) Schematic of a modified side-illumination EC-TERS setup with an air objective. (*c*) Schematic showing a side-illumination EC-TERS setup with a water-immersion objective. (*e*) Schematic of a bottom-illumination EC-TERS setup with an oil-immersion objective (40). Panel *e* adapted from Reference 40 with permission; copyright 2015 American Chemical Society. (*g*) Schematic showing a top-illumination EC-TERS setup with a water-immersion objective (47). Panel *g* adapted from Reference 47 with permission; copyright 2019 Elsevier. Abbreviations: AFM, atomic force microscope; CE, counter electrode; EC-TERS, electrochemical tip-enhanced Raman spectroscopy; NA, numerical aperture; RE, reference electrode; STM, scanning tunneling microscope; WE, working electrode; XYZ, three axes.

of light it blocks. The advantages of this configuration are that the influence of the curved liquid surface in the focused optical path was avoided, and the liquid layer thickness in the optical path was reduced to ~1 mm to reduce the optical distortion. As a result, the tip apex was clearly observed in optical microscopy, and the laser spot was well-focused onto the tip apex. This configuration was adapted later by the Kim group (41) for characterizing the oxidative desorption of a self-assembled monolayer of thiophenol (TP) on Au(111).

However, the optical distortion still was not completely eliminated in this configuration. The bottom-illumination configuration was a more effective way to decrease the optical distortion. In this configuration, the laser was focused from the bottom to illuminate the tip apex, which eliminates the need for it to pass through the thick electrolyte layer (**Figure 2*d***). The Van Duyne group (40) developed EC-AFM-TERS (electrochemical atomic force microscopy tip-enhanced Raman spectroscopy) based on the bottom-illumination configuration (**Figure 2*e***). Because the Raman optics were located on the opposite side of the cell from the EC-SPM component, there was a large open space, which allowed the use of an oil-immersion objective with a high NA (~1.4) to improve the excitation and collection efficiency. This enabled the probing of the nanoscale redox behavior of a few Nile blue (NB) molecules on a transparent indium tin oxide (ITO) electrode. However, the transmission configuration cannot be used to study opaque electrodes, such as single-crystal metal electrodes, which are important in electrochemistry. Therefore, further improving the

performance of EC-TERS setups based on the side-illumination or top-illumination configuration is still quite important.

Thereafter, both the Domke group (42) and the Van Duyne group (43) developed the side-illumination EC-TERS setup with air objectives. To reduce the optical distortion, the Domke group (44) adapted a spatial light modulator to modulate the phase of the excitation light to correct the optical distortion. Recently, our group (45) introduced a water-immersion objective with a short working distance and a high NA (0.8) into the side-illumination EC-TERS setup (**Figure 2*c***). The air in the gap between the objective and the glass window was replaced by a droplet of water. Thus, the mismatch between the refractive indices of different media was effectively decreased and the optical distortion largely eliminated by using the water-immersion objective (46). Due to the high NA and elimination of the optical distortion, the sensitivity was improved fivefold compared with our first-generation EC-TERS setup. In the same year, the Maisonhaute group (47) developed a top-illumination EC-TERS setup based on a water-immersion objective (**Figure 2*g***) in which the objective is vertically immersed in the electrolyte solution. With this setup, they demonstrated the 8-nm-resolution EC-TERS imaging of an Au surface functionalized with azobenzenethiol derivatives. To accommodate the objective with a short working distance, a special tip holder was designed to bring the TERS tip into the focal point of the objective at a 45° angle. Such a design eliminates the air–liquid interface in the optical path and has no optical distortion. More recently, we also developed an AFM-based top-illumination EC-TERS setup with a water-immersion objective to eliminate optical distortion and achieved a high detection sensitivity (48). Compared with the side-illumination setup, the top-illumination configuration provides better microscopic imaging quality due to its normal incidence and symmetrical focus on the sample, making it more convenient to observe the electrode surface and the laser spot. The side- and top-illumination EC-TERS setups using water-immersion objectives are applicable to opaque electrodes with no optical distortion and improved sensitivity, and thus empower EC-TERS for in situ nanoscale characterization and exploration of more important electrochemical systems.

In addition to the specially designed optical configuration, the electrochemical potential should be properly controlled in the EC-TERS setup. Until now, EC-TERS has been based on either EC-STM or EC-AFM. In EC-AFM-TERS, only the electrode potential of the substrate needs to be controlled. Therefore, a standard three-electrode system can be used, with a potentiostat controlling the potential of the substrate [as the working electrode (WE)] versus the reference electrode (RE) in EC-AFM-TERS. However, in the EC-STM-TERS setup, both the tip and the substrate potentials need to be controlled. Therefore, it requires a four-electrode [substrate, tip, RE, and counter electrode (CE)] electrochemical system and a bipotentiostat to independently control the potentials of the tip and the substrate versus the RE. The bias is determined by the potential difference between the tip and the substrate. The currents on the substrate and tip can be independently measured by the bipotentiostat. Because all of the currents (including the tunneling, charging, and Faradaic currents) flowing through the tip are amplified by the STM current preamplifier and used as the STM feedback, the tip needs to be insulated to reduce the charging and Faradaic currents, so that they are much smaller than the tunneling current. In this way, the charging and Faradaic currents do not interfere with the STM feedback.

2.2. Tip-Related Issues

The tip is the core of TERS in air, vacuum, and liquid conditions. Generally, STM-TERS tips are fabricated by the electrochemical etching of Au or Ag wires (49–51). AFM-TERS tips are fabricated by depositing a layer of Au or Ag metallic film on commercial AFM tips with vacuum (52–54), electrochemical (55, 56), or chemical (57, 58) deposition methods. The geometrical

Table 1 Tip-related issues in EC-TERS

Characteristic	EC-STM-TERS tips	EC-AFM-TERS tips
Fabrication methods	Electrochemical etching	Vacuum deposition Chemical deposition Electrochemical deposition
Tip insulation	Required	Not required
Insulation materials	Polyethylene glue Paraffin wax Zapon Nail polish	NA
Prevention of delamination	NA	Buffer layer: SiO_x or Cr–Au Dielectric material coating layer: Al_2O_3 (applicable in neutral solution), SiO_2 (pH < 10) ZrO_2 (pH 3.6–12.6)
Prevention of contamination	Dielectric material coating Assembled with thiols	
LSPR position tuning	Dielectric material coating Refractive index modification FIB milling	

Abbreviations: EC-AFM-TERS, electrochemical atomic force microscopy tip-enhanced Raman spectroscopy; EC-STM-TERS, electrochemical scanning tunneling microscopy tip-enhanced Raman spectroscopy; EC-TERS, electrochemical tip-enhanced Raman spectroscopy; FIB, focused ion beam; LSPR, localized surface plasmon resonance; NA, not applicable.

parameters of the tip apex play important roles in determining the enhancement factor. Related issues in the preparation of TERS tips and the use of the TERS tip under the conventional air condition have been discussed in detail in our previous reviews (59, 60). Here we focus on their use in EC-TERS (**Table 1**).

2.2.1. Insulation for EC-STM-TERS tips. In EC-STM-TERS, the tip needs to be insulated to minimize the interference of the Faradaic and charging currents with the tunneling current. Although insulation methods are mature for EC-STM tips, there are additional requirements for EC-STM-TERS tips. The insulation materials should be Raman and fluorescence inactive and under laser illumination should not produce any spectral signals that interfere with the TERS signal. In addition, the insulation layer should be stable and not swell in the electrolyte during long-term EC-TERS experiments. Therefore, the properties and the quality of the insulation layer are important. Previously, polyethylene glue (39), Zapon (42, 47), paraffin wax (41), and nail polish (61–64) have been successfully used as insulation materials for EC-STM-TERS tips. A typical method used to obtain an insulated TERS tip is to push a metallic tip through a liquified insulation material. The liquified materials attach to the surface of the tip (**Figure 3*a***) and withdraw from the tip apex due to surface tension (39). This process usually needs to be repeated from one to three times, depending on the material, to ensure that most of the surface area of the tip except for the apex has been effectively insulated. After the insulation procedure, the exposed area can be determined with cyclic voltammetry (CV) by mathematically describing the tip as a conic ultramicroelectrode (41) (see Section 2.3.1).

2.2.2. Improving the stability of metal coatings for EC-AFM-TERS tips. The metallic layer of an AFM-TERS tip easily delaminates when the tip is working in solution due to the weak binding force between the metallic layer and the AFM tip. In addition, the morphology of the

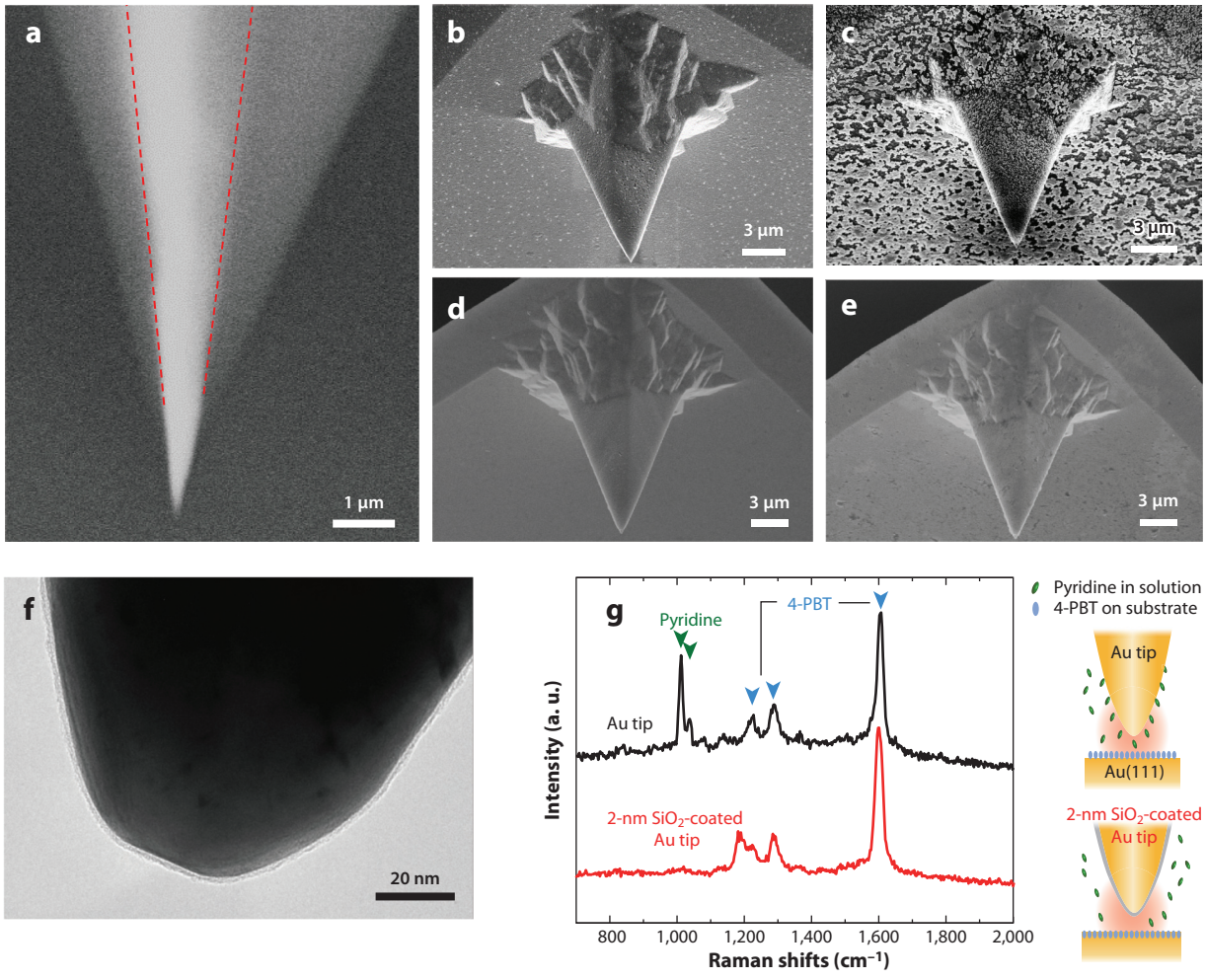

Figure 3

(*a*) SEM image of an STM-TERS tip after insulation. The dotted red lines indicate the boundary between the Au tip and the coated polymer film. Panel *a* adapted with permission from Reference 39; copyright 2015 American Chemical Society. (*b*,*c*) SEM images of an Ag-coated tip before and after immersion in water. (*d*,*e*) SEM images of a Cr–Au–Ag–coated AFM-TERS tip before and after immersion in water. Panels *b*–*e* adapted with permission from Reference 66; copyright 2018 Royal Society of Chemistry. (*f*) Transmission electron microscopy image of a pinhole-free shell-coated tip. The thickness of the SiO_2 coating was ~2 nm. (*g*) TERS spectra of 4-PBT assembled on Au(111) acquired by a bare STM-Au tip (*black line*) and an SiO_2-coated STM-Au tip (*red line*) in an electrolyte solution containing 10-mM $NaClO_4$ and 5-mM pyridine. Panels *f* and *g* adapted with permission from Reference 69; copyright 2018 John Wiley & Sons. Abbreviations: 4-PBT, 4′-[(pyridin-4-yl)biphenyl-4-yl]methanethiol; AFM-TERS, atomic force microscopy tip-enhanced Raman spectroscopy; SEM, scanning electron microscopy; STM-TERS, scanning tunneling microscopy tip-enhanced Raman spectroscopy; TERS, tip-enhanced Raman spectroscopy.

apex may be altered by the high-frequency (~100 kHz) vibration that occurs during tapping mode operation in solution, leading to a dramatic decrease in the TERS enhancement. Therefore, the mechanical stability of the metallic coating films needs to be improved for EC-AFM-TERS tips.

Two strategies may be used to accomplish this. One is to strengthen the adhesion of the metallic coating on the AFM tips by precoating the AFM Si tips with a buffer layer of SiO_x (65) or Cr–Au (66). This prevents the coating layer from peeling off when the tip is working in solution

(**Figure 3*b–e***). The other method is to deposit a protective layer of a dielectric material, such as SiO_2, Al_2O_3, or ZrO_2, over the Au or Ag coatings with the wet-chemistry or atomic layer deposition (ALD) method to effectively improve the stability of the metallic coating layers in liquid. However, the protective layer inevitably increases the gap between the tip and the sample and so sacrifices the TERS enhancement. Therefore, a delicate balance needs to be found between effective protection and maintaining high enhancement. In addition, the applicable pH range of the protective dielectric layers should be taken into consideration in the EC-TERS experiment. Due to the dissolution of Al_2O_3 in acidic and basic solutions, an Al_2O_3-protected tip is applicable only in neutral electrolyte solution. Tips coated with SiO_2 via ALD can be used in electrolyte solutions with pH < 10 (67). Tips coated with ZrO_2 by the wet-chemistry process (68) can be used over a broad pH range from 3.6 to 12.6 (67).

All of these methods can effectively prevent the metallic coating from peeling off of AFM-TERS tips when they are working in contact mode in solution. However, to the best of our knowledge, there is still no method that can effectively prevent the degradation at the tip apex in the tapping mode caused by the strong interaction between the tip and solution under high-frequency vibration. Therefore, protection methods need to be further developed to extend the EC-AFM-TERS method to work in tapping mode.

2.2.3. Preventing the adsorption of contaminants on the tips. To date, EC-TERS has been performed in simple electrolyte solutions that contain only supporting electrolytes with a weak adsorption ability and have small Raman scattering cross sections that do not interfere with TERS measurements. However, in many practical electrochemical systems, the solution contains analyte molecules or other complex components. These species in the solution may adsorb on the TERS tips and give rise to enhanced Raman signals, which may interfere with the TERS spectra of the target molecules. One effective solution is to deposit ultrathin and pinhole-free dielectric materials on the tip (**Figure 3*f***), as mentioned in Section 2.2.2 (69). The pinhole-free dielectric coating can effectively prevent the adsorption of molecules and suppress their interference with the detection of the species of interest on the substrate surface (**Figure 3*g***). An alternative solution is to assemble a layer of molecules on the tip that have small Raman scattering cross sections but stronger interactions with the metallic surface than with the species in the solution, such as ethanethiol (65). By properly designing the surface functional groups, this assembled layer can inhibit the adsorption of molecules and contamination. These methods could allow the application of EC-TERS to more complex electrochemical systems.

2.2.4. Variation of the localized surface plasmon resonance position. As mentioned in Section 1, the field enhancement of TERS mainly originates from the LSPR effect. When the environment is changed from air to water, the dielectric constant of the medium increases, which causes a notable red shift of the LSPR peaks (70). Taking a single Au or Ag nanoparticle for an example, there is approximately a 40–60-nm red shift for Ag (71, 72) and a 60–80-nm red shift for Au (73) upon changing the environment from air to liquid. The red shift of the tip LSPR in liquid may lead to a shift away from the optimal wavelength obtained in air and a decrease in the TERS sensitivity. To solve this problem, one method used is to change the laser wavelength to match the LSPR position in solution. However, this requires a Raman system with tunable excitation wavelengths. The other method is to tune the LSPR position of the TERS tip by various methods, including coating with some dielectric materials (74) or refractive index modification (75). Recently, a focused ion beam has increasingly been used to precisely modify the tip length (76) as well as to mill the tip with some special structures (77–79) to tune the LSPR position. Furthermore, with the help of numerical simulation methods, it is now possible to simulate the

optical response and electromagnetic field of the TERS tip and tip-substrate system to guide the optimization of the experimental parameters of EC-TERS tips.

2.3. Experimental Guidelines for EC-TERS

Successful EC-TERS experimentation requires careful, delicate, and skillful operation to obtain reliable EC-TERS spectra of probed species. This section provides the important operational steps and details that may determine the success of EC-TERS experiments.

2.3.1. Characterization of the tip properties. For EC-STM-TERS tips, the quality of tip insulation should be checked by CV measurement. The exposed area of the tip after insulation can be considered to be an ultramicroelectrode with a conical shape. The size of the exposed apex can be estimated from the Faradaic current using the standard electrochemical redox [$Fe(CN)_6^{3-}/Fe(CN)_6^{4-}$ or $Ru(NH)_6^{3+}/Ru(NH)_6^{2+}$] solutions and the formula $r = \sqrt{\frac{I}{FDC}}$. Here, r is the radius of the ultramicroelectrode and I, F, C, and D are the steady-state current obtained from CV, Faraday's constant, the concentration, and the diffusion coefficient of the redox couple, respectively. Before the EC-TERS measurement, the electrochemical response of the tip in the practical electrolyte solution should be tested to obtain the potential window of the tip and the substrate that can be applied in the EC-TERS measurement. Generally, the tip should be kept within the potential range in which the electrochemical current of the tip is one order of magnitude smaller than the set point of the tunneling current. For the EC-AFM-TERS tip, the performance of the tip after coating with the protection layer should be checked. Usually EC-TERS experiments (especially mapping) are time-consuming, so the long-term stability and enhancement of the AFM-TERS tip in the electrolyte need to be checked under the working conditions. Above all, only tips with high stability and high enhancement can be used for EC-TERS experiments.

2.3.2. Protection of the scanning probe microscopy unit and objective. In EC-TERS experiments, the tip holder and the water-immersion objective may be immersed in the electrolyte solution. The electrolyte and evaporated solutions may corrode the SPM unit and the objective. Therefore, important SPM components need to be coated with protective materials to prevent corrosion by the electrolyte. The water-immersion objective should be carefully covered with a thin, soft, and optically transparent polyethylene film to protect the objective while maintaining the excellent optical properties of the objective. During EC-TERS experiments, extra care must be taken to avoid spillage and leakage of the electrolyte solution, which can corrode the instrument.

2.3.3. Modulation of the potential. In the EC-STM-TERS experiment, there are two methods of setting the potentials of the sample and tip. One method is to fix the tip potential while modulating the sample potential. In this way, the bias is changed with varied sample potentials, which can lead to a change in the gap distance and the plasmonic coupling between the tip and substrate. As a result, however, this method may lead to variation in the TERS intensity. The other method is to fix the bias while modulating the sample potential. This strategy can maintain the distance between the tip and substrate, avoiding variation of the TERS intensity during modulation. In the EC-AFM-TERS experiment, the potential is applied only to the substrate, and considering the influence of the tip potential on the system is not necessary.

2.3.4. Methods to check the reliability of EC-TERS spectra. Due to the small distance between the tip and the sample in EC-TERS (from subnanometer to a few nanometers), instability in the TERS setup and the environmental vibrations can cause the transfer of molecules from the

substrate to the tip, which contaminates the tip. It is crucial to double-check that the Raman signals are actually from the molecules adsorbed on the substrate surface so that the obtained TERS spectra reflect the true behavior of surface species on the probed substrate electrode (60). A reliable method for checking the cleanliness of the tip and the reliability of EC-TERS spectra is to perform a TERS measurement on a clean substrate with the same tip following the EC-TERS measurement. For EC-STM-TERS, a more convenient strategy is to monitor the TERS spectra upon changing the potential of either the tip or the sample. If the molecular behavior is sensitive only to the modulation of the tip potential, this indicates that the tip is contaminated.

3. APPLICATIONS OF EC-TERS

3.1. Probing Molecular Adsorption and Molecular Structure

In the first demonstration of EC-TERS, this technique was found to be more sensitive than EC-SERS to subtle changes in the molecular configuration at the electrochemical interface (39). **Figure 4*a–d*** shows a comparison of the EC-TERS spectra of 4′-[(pyridin-4-yl)biphenyl-4-yl]methanethiol (4-PBT) assembled on an Au(111) surface and EC-SERS spectra of the same molecule on Au nanoparticles (NPs). In the EC-TERS spectra, the doublet peaks at 1,592 cm^{-1} (vibration of the pyridine ring) and 1,605 cm^{-1} (vibration of the benzene ring) were observed at 0.3 V (**Figure 4*a***). When the potential was moved to −0.7 V, the 1,592 cm^{-1} peak blue-shifted to overlap with the 1,605 cm^{-1} peak and appeared as a single peak after the pyridine ring was protonated (**Figure 4*b***). However, such a potential-dependent spectral change due to molecular protonation and deprotonation was not observable in EC-SERS spectra (**Figure 4*c***). The main reason is that double-end-bonded 4-PBT molecules can easily form among Au NPs in the SERS configuration (**Figure 4*d***), which may interfere with the formation of protonated species. This work demonstrates how the well-defined configuration makes EC-TERS a reliable method for probing molecular structure changes at the electrochemical interface.

The Domke group (80) employed EC-TERS to study the molecular adsorption geometry as well as the protonation process on atomically flat Au(111) electrodes as a function of the applied potential (**Figure 4*e–g***). Generally, vibrational modes with a component parallel to the direction of the surface electrical field can be effectively enhanced. On the basis of the surface selection rule and the polarizability anisotropies of the Raman tensors, the decrease of intensities of the 736 cm^{-1} peak (ring breathing) and the 1,464 cm^{-1} peak (N–C stretch, C–H bend, and NH_2 scissors) with the positive shift of the potential (**Figure 4*e***) can reflect the reorientation of adsorbed adenines from tilted to upright to flat with respect to the Au(111) surface. However, the peak frequencies of the above vibrational modes are sensitive to the molecule-ion interaction (**Figure 4*f***), which can reflect the molecular transitions between protonated, neutral, and partially positive charged states. In addition, the peak at 260 cm^{-1} (Au–N mode) can provide a wealth of information on the adsorbate–electrode interaction. The blue shift of this mode with the positive-shifted potential reveals a strengthening of the Au–N bond due to an increased donation of the N lone pairs of the deprotonated adenine adsorbate to the Au d-band. Because of the well-defined configuration and the rich chemical information, EC-TERS is particularly promising in probing the molecular structure and adsorption configuration of the adsorbate at the electrochemical interface. With nanoscale spatial resolution, nanoscale spectral imaging of an electrochemical interface can be used to reveal the relationship between the surface structure and molecular behavior.

3.2. Characterization of Electrochemical Reactions

In situ monitoring of the evolution of the chemical structure of reaction-related species with nanometer-scale resolution during the electrochemical reaction would help to reveal the

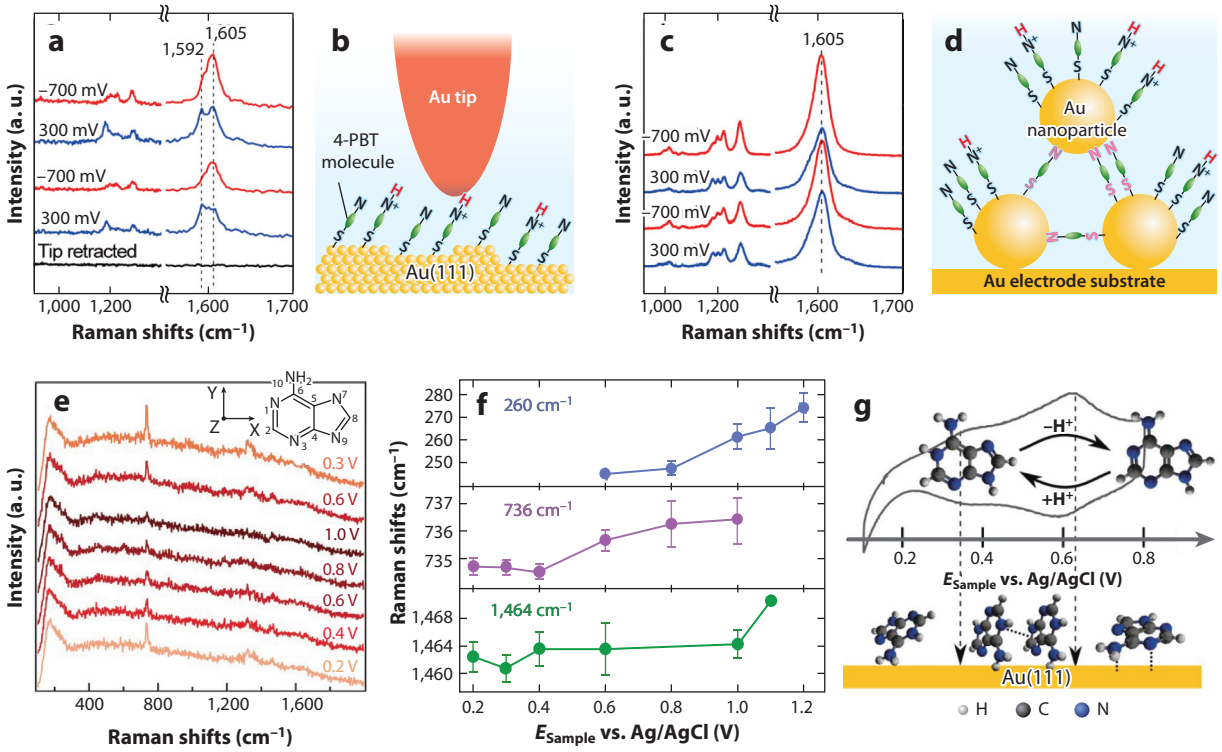

Figure 4

(*a*) Graph showing potential-dependent TERS spectra of 4-PBT molecules adsorbed on an Au(111) electrode surface in 0.1-M $NaClO_4$ (pH 10). (*b*) Schematic illustration of the TERS configuration for studying the protonation of 4-PBT. (*c*) Graph of potential-dependent SERS spectra of 4-PBT molecules adsorbed on an Au NP surface in 0.1-M $NaClO_4$ (pH 10). (*d*) Schematic of the SERS configuration for studying the protonation of 4-PBT. Elements shown in pink letters are double-end bonding to the Au NPs. Panels *a–d* adapted with permission from Reference 39; copyright 2015 American Chemical Society. (*e*) Graph of potential-dependent TERS spectra of adenine adsorbed on an Au(111) electrode surface in 0.01-M H_2SO_4. The inset shows the molecular structure of adenine. (*f*) Graphs of fitted peak positions of the 260 cm^{-1} (*blue*), 736 cm^{-1} (*purple*), and 1,464 cm^{-1} (*green*) peaks as a function of the potential of the Au(111) substrate. (*g*) Schematic of the potential-dependent reversible adsorption and protonation of adenine on Au(111) within the potential window of cyclic voltammetry. The dashed arrows clearly divide the potential axis into three segments, indicating the different adsorption configurations in corresponding potential regions. Panels *e–g* adapted with permission from Reference 80; copyright 2017 John Wiley & Sons. Abbreviations: 4-PBT, 4′-[(pyridin-4-yl)biphenyl-4-yl]methanethiol; NP, nanoparticle; SERS, surface-enhanced Raman spectroscopy; TERS, tip-enhanced Raman spectroscopy.

reaction mechanism and further shed light on the structure-function relationship in electrocatalysis. Due to its high spatial resolution and ability to provide rich chemical information, EC-TERS is a promising in situ tool for investigating the heterogeneous behaviors of reactants and electrocatalysts.

EC-TERS was used to monitor the nanoscale electrochemical redox behavior of NB molecules on an ITO electrode (**Figure 5*a–c***) (40, 81, 82). When the potential was moved from 0 V to −0.6 V, the TERS intensities greatly decreased as a result of the transformation of NB from the resonant to the nonresonant state, owing to the reduction of the NB molecules (**Figure 5*a***). At a low coverage, a steplike feature in the TERS intensity-potential curve (termed a TERS voltammogram) was observed (**Figure 5*b,c***) that corresponds to the reduction and oxidation of a few molecules or even a single molecule. In addition, the formal potential E^0 in the TERS voltammograms differed on different sites, indicating the nanoscale heterogeneity of the reaction behavior on the polycrystalline

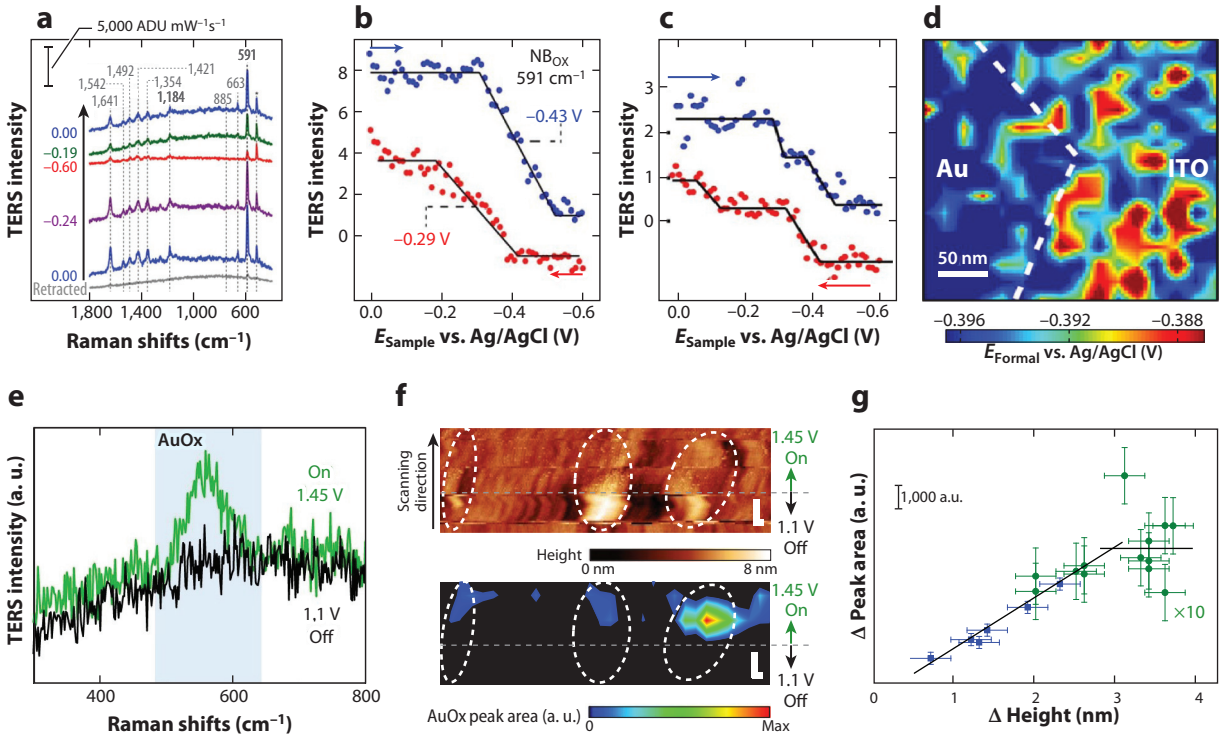

Figure 5

(*a*) Graph showing EC-TERS spectra of adsorbed NB on ITO acquired at different potentials. (*b*,*c*) TERS voltammograms at different positions using the 591-cm^{-1} intensity versus applied potentials. Surface coverages beneath the tip are tens of molecules in panel *b* and a few molecules or a single molecule in panel *c*, respectively. Panels *a*–*c* adapted with permission from Reference 40; copyright 2015 American Chemical Society. (*d*) Reconstructed formal potential E_{Formal} map of an Au nanoplate on ITO. The white dashed line indicates the boundary between the Au nanoplate and ITO. Panel *d* adapted with permission from Reference 83; copyright 2019 American Chemical Society. (*e*) Graph showing EC-TERS spectra of defects on Au(111) at 1.1 V (*black*) and 1.45 V (*green*) versus Pd–H. The blue background highlights the peak area of the Au oxide. (*f*, *top*) EC-STM and (*bottom*) EC-TERS images of the same area. The black arrow shows the direction of scanning and the straight white dotted lines separate the lower part, corresponding to a potential of 1.1 V, from the upper part, corresponding to 1.45 V. The white dotted circles indicate defects on Au(111). The white L-shaped bars indicate the scale in the horizontal and vertical directions; the scale bars equal 10 nm. (*g*) Graph of AuOx peak area versus defect height on different defects. Data sets shown in blue and green were obtained by different tips on different samples. Panels *e*–*g* adapted with permission from Reference 84; copyright 2019 Springer Nature. Abbreviations: ADU, analog-to-digital unit; EC-STM, electrochemical scanning tunneling microscopy; EC-TERS, electrochemical tip-enhanced Raman spectroscopy; ITO, indium tin oxide; NB, Nile blue; TERS, tip-enhanced Raman spectroscopy.

ITO. To spatially resolve the heterogeneity of the reduction behavior of NB, EC-TERS mapping was performed at the boundary between a 20-nm-thick Au(111) nanoplate and an ITO substrate surface with a spatial resolution of about 40 nm (83). The formal potential E^0 was extracted from the fitting of the TERS voltammogram at each site to construct the reactivity distribution over the electrode surface (**Figure 5*d***). The mapping result clearly shows that the E^0 is more negative at sites on Au than it is on ITO, indicating a higher reactivity on ITO. The statistical analysis of the site-dependent E^0 on Au and ITO further confirmed this result. Interestingly, the reactivity difference of the nanograins on ITO could be resolved by a direct comparison of the E^0 and the AFM friction image. Such site-specific reactivity information with nanoscale spatial and few-mV energy resolutions is not achievable by using conventional spectroelectrochemical methods.

In addition to molecular reactants, it was found that the active sites of electrocatalysts may also undergo chemical conversions during the electrochemical reaction. For example, recently the Domke group (84) implemented EC-STM-TERS to monitor the oxidation reaction of Au nanodefects on Au(111) before the oxygen evolution reaction with 10-nm spatial resolution. Two Raman peaks related to the Au oxidation (Au_2O, >565 cm^{-1}; Au_2O_3, <565 cm^{-1}) (**Figure 5*e***) can be obtained only at the defect sites of Au(111) after applying a positive oxidation potential to the electrode (1.45 V versus Pd–H) (**Figure 5*f***). Furthermore, the maximum depth (about 3 nm) of AuOx at the defects was obtained by linear correlation of the intensity of the EC-TERS spectra with the height of the nanodefects (**Figure 5*g***). These results clearly reveal that defects on Au(111) are the electrocatalytically active sites during the Au oxidation reaction and further demonstrate that EC-TERS is a promising in situ tool to monitor the chemical transformation of catalytically active sites.

3.3. Characterization of Photoelectrochemical Reactions

The surface plasmon (SP) in the EC-TERS configuration could be used not only to enhance the Raman scattering process but also to simultaneously drive the SP-assisted photochemical reactions. Therefore, EC-TERS is an ideal tool for the in situ characterization of the SP-assisted photochemical reaction. In addition, EC-TERS provides flexible electrochemical control of the electronic and chemical properties of catalysts, making this technique a potential method to study the synergistic effect of SP and electrochemistry on reactions at the nanometer scale.

Recently, we used EC-TERS to monitor in situ an SP-driven decarboxylation reaction at the nanoscale and resolve the spatial distribution of reactive hot carriers beneath the plasmonic tip (**Figure 6**) (85). The time-series TERS spectra (**Figure 6*a***) show that the feature peaks (998 cm^{-1} and 1,020 cm^{-1}) of TP gradually appeared after the TERS tip approached the 4-mercaptobenzoic acid (4-MBA)-adsorbed Au(111) electrode, demonstrating that the 4-MBA molecules beneath the plasmonic tip had been converted to TP. The potential-dependent TERS spectra indicate that the decarboxylation reaction was promoted by the positive shift of the potential from -0.7 V to -0.4 V (**Figure 6*b***) due to the elevation of the energies of hot holes. Because the decarboxylation reaction is irreversible, the feature peak of TP remained even when the potential was returned to -0.7 V. In this way, we could flexibly modulate the electrode potential to turn on (before TERS mapping) or turn off (during TERS mapping) the SP-driven reaction. Thus, we took advantage of the nanoscale resolution of EC-TERS to visualize the SP-induced reaction region without further perturbing the reaction during TERS mapping. On considering that the reaction profile depends on the initial distribution of the hot carriers generated by the localized plasmonic electrical field and the carrier transport, which follows an exponential decay function (**Figure 6*c***), we obtained the transport distance of the reactive plasmonic hot carriers in real space ($\sim$20 nm) from the experimentally obtained reaction profile. Furthermore, we found that the profile of the reaction induced at the negative potential is narrower (**Figure 6*d***), which indicates that the hot holes with higher energies could be collected only within a shorter distance. These conclusions could guide the development of SP-assisted photocatalysts by encouraging designs that arrange the reactant molecules within the transport distance of reactive hot carriers to efficiently collect and utilize them. This work shows the unique advantages of EC-TERS in the characterization of SP-assisted photoelectrocatalysis. With further improvements in sensitivity, EC-TERS will be able to address more interesting and challenging issues in photoelectrocatalytic systems, including probing the distribution of hot carriers in metal-semiconductor composite photoelectrocatalysts and identifying the active sites in complicated photoelectrocatalysts.

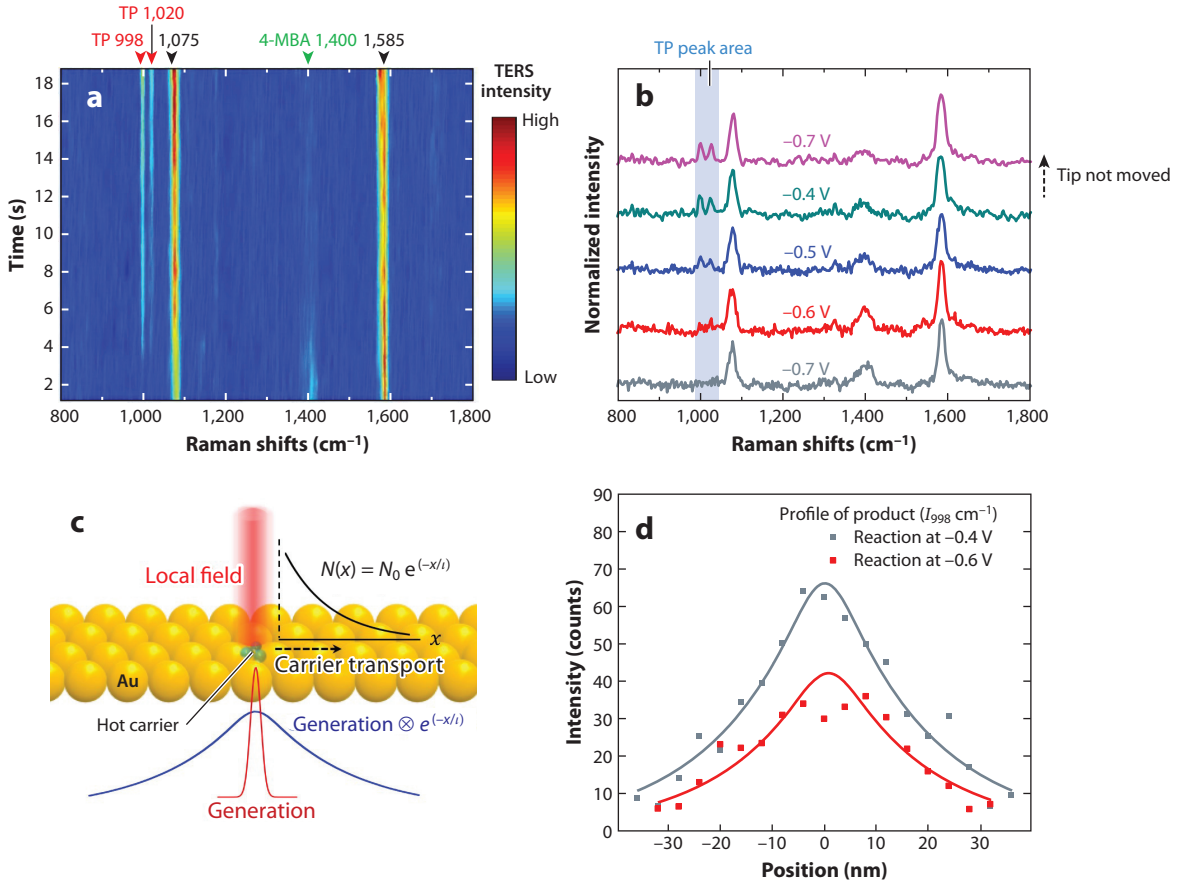

Figure 6

(*a*) Graph of the time-series TERS spectra obtained in 0.1-M $NaClO_4$ (pH 10) after a TERS tip approached an Au(111) surface coated in 4-MBA. The numbers on top of the graph indicate the peak position. The abbreviations TP and 4-MBA indicate the origins of the peaks. (*b*) Graph showing the potential-dependent TERS spectra of 4-MBA. The dashed arrow highlights that the potential is moved from −0.4 V (*green spectrum*) to −0.7 V (*purple spectrum*) while the tip is not moved. (*c*) Schematic illustration of hot carrier generation and transport on the surface. The initial generation distribution of the hot carriers follows the localized plasmonic electrical field, and the carrier transport follows an exponential decay function. Iota (ι) is the transport distance of the hot carriers. N is the number of hot carriers. N_0 and $N(x)$ are the number of hot carriers at the generated site and at the site after transporting for a distance of x, respectively. The red curve indicates the initial profile of hot carriers generated by the localized plasmonic electrical field. The blue curve indicates the overall distribution of hot carriers after transport. (*d*) Graph of profiles of the reaction induced at −0.6 V (*red*) and −0.4 V (*gray*). The lines were fitted using the model in panel *c*. The fitted transport distances of reactive hot holes are ∼17 nm at −0.6 V and ∼20 nm at −0.4 V. Abbreviations: 4-MBA, 4-mercaptobenzoic acid; TERS, tip-enhanced Raman spectroscopy; TP, thiophenol. Figure adapted with permission from Reference 85; copyright 2020 Springer Nature.

4. SUMMARY AND OUTLOOK

At present, TERS is the only nanospectroscopy technique capable of working in electrochemical conditions; this provides a unique advantage over nano-IR, which is hampered by the interference of water. The inherent advantages of EC-TERS, that is, nanoscale spatial resolution and rich chemical information, make it a powerful technique for studying electrochemical interfaces, in particular correlating the electrochemical activity of specific sites on a surface with their nanoscale structures. However, due to the limited enhancement and reproducibility of fabricating

tips, EC-TERS is mainly applied to the study of some basic and model systems on an Au or Ag substrate. Once these bottleneck problems are tackled in the near future, the development and application of EC-TERS to various fields ranging from fundamental research to industrial applications, such as electrocatalysis, photovoltaics, and fuel cell and lithium ion batteries, will be boosted.

In the following, we discuss challenges and opportunities within the issues of tips, sensitivity, and time resolution.

1. **TERS tips**. Even after 20 years' development, the TERS tip is still the key determining factor for TERS, as it plays the dual roles of providing both high-resolution morphological information on the surface and enhanced Raman signals. At present, fabricating highly active TERS tips with high reproducibility is still a great challenge, which hampers TERS from becoming a standard analytical tool (59). Further work in this field is needed to develop microfabrication methods that allow the batch production of TERS tips with high reproducibility. Alternatively, focused ion beam (78, 79, 86, 87) or field-directed sputtering sharpening (88) can be used to finely modify the radii and geometry of the tip apex, ensuring both high TERS activity and high reproducibility. It is also important to combine efficient techniques for in situ monitoring of the optical response of the tip, so that it can provide feedback to guide the fabrication process and improve reproducibility (89).
2. **Sensitivity**. Though EC-TERS has demonstrated its ability to observe single-molecule behavior, the pursuit of higher sensitivity has never stopped. As most (EC-)TERS measurements rely on an Au or Ag substrate that can effectively couple with the tip to provide strong enhancement, developing single tips with ultrastrong plasmonic enhancement is important to achieving noncoupling mode (EC-)TERS. With this, the application of (EC-)TERS could be extended to more general systems in the fields of energy, materials, and biology without the use of an Au or Ag substrate to provide plasmonic coupling. The realization of such a tip requires a comprehensive design for both the optics and the microstructure or nanostructure of the tip, which requires close collaboration between physicists and chemists. Nonlinear Raman effects whose intensity increases nonlinearly with increased laser power, such as stimulated Raman scattering, can also be introduced to enhance the Raman signal (90). Another potential solution to improve the sensitivity is to adsorb reporter Raman molecules on the tip to indirectly sense the chemical changes above specific sites (91). This indirect strategy is especially powerful when the pH and temperature at the reaction sites change with the electrochemical reactions.
3. **Time-resolved (EC-)TERS**. The ultimate goal of the electrochemistry and surface science communities is to monitor the dynamics of chemical reactions at a specific site to reveal the reaction mechanism. With specially designed detection systems, the time resolution for SERS has reached milliseconds (92) and even microseconds. However, sensitivity is still the bottleneck issue for using TERS to acquire Raman signals with a reasonable signal-to-noise ratio in an ultrashort time. Introducing ultrafast optics to TERS would simultaneously enable nanoscale spatial resolution and ultrafast time resolution.
4. **Operando analysis**. A TERS setup has already been installed in a glove box to ex situ probe the nanoscale composition of the solid electrolyte interphase on a silicon anode after galvanostatic cycling of a Li-ion battery (93). However, more interesting would be to perform EC-TERS measurements in a glove box or other atmosphere-controlled environment for the operando study of the reaction processes of batteries as well as other electrocatalytic systems. This can be achieved by further improvement in the design of optics and spectroelectrochemical cells as well as optimization of the experimental protocol.

5. **Combination with other techniques**. (EC-)TERS can provide chemical information on surface species, and it will be able to accurately correlate the chemical, physical, and electrochemical properties of different sites on the surface if it can be combined with such techniques as Kelvin probe force microscopy, scanning electrochemical microscopy, and others. As a result, it will be possible to clarify the relationships between the structure, properties, and performance of some important electrochemical systems with heterogeneous structures including bimetallic materials, two-dimensional materials, and metal-semiconductor composite electrocatalysts.

DISCLOSURE STATEMENT

The authors are not aware of any affiliations, memberships, funding, or financial holdings that might be perceived as affecting the objectivity of this review.

ACKNOWLEDGMENTS

The authors acknowledge financial support from the National Natural Science Foundation of China (NSFC) (grants 21633005, 21790354, and 22021001) and the Ministry of Science and Technology (MOST) of China (grant 2016YFA0200601).

LITERATURE CITED

1. Bard AJ, Faulkner LR. 2001. *Electrochemical Methods: Fundamentals and Applications*. New York: John Wiley & Sons
2. Kuwana T, Darlington RK, Leedy DW. 1964. Electrochemical studies using conducting glass indicator electrodes. *Anal. Chem.* 36:2023–25
3. Mizoguchi T, Adams RN. 1962. Anodic oxidation studies of N,N-dimethylaniline. I. Voltammetric and spectroscopic investigations at platinum electrodes. *J. Am. Chem. Soc.* 84:2058–61
4. Mark HB, Pons BS. 1966. An *in situ* spectrophotometric method for observing the infrared spectra of species at the electrode surface during electrolysis. *Anal. Chem.* 38:119–21
5. Fleischmann M, Hendra PJ, McQuillan AJ. 1974. Raman spectra of pyridine adsorbed at a silver electrode. *Chem. Phys. Lett.* 26:163–66
6. Guyot-Sionnest P, Tadjeddine A. 1990. Spectroscopic investigations of adsorbates at the metal-electrolyte interface using sum frequency generation. *Chem. Phys. Lett.* 172:341–45
7. Tourillon G, Dartyge E, Dexpert H, Fontaine A, Jucha A, et al. 1985. Electrochemical inclusion of metallic clusters in organic conducting polymers: an in situ dispersive X-ray absorption study. *Surf. Sci.* 156:536–47
8. Antonio MR, Soderholm L, Song I. 1997. Design of spectroelectrochemical cell for in situ X-ray absorption fine structure measurements of bulk solution species. *J. Appl. Electrochem.* 27:784–92
9. Fleischmann M, Oliver A, Robinson J. 1986. *In situ* X-ray diffraction studies of electrode solution interfaces. *Electrochim. Acta* 31:899–906
10. Masuda T, Kondo T. 2019. New sights into the electrochemical interface provided by *in situ* X-ray absorption fine structure and surface X-ray scattering. *Curr. Opin. Electrochem.* 14:81–88
11. Turrell G, Corset J. 1996. *Raman Spectroscopy: Development and Applications*. London: Academic
12. Smith E, Dent G. 2005. *Modern Raman Spectroscopy—A Practical Approach*. Chichester, UK: John Wiley & Sons
13. Jeanmaire DL, Van Duyne RP. 1977. Surface Raman spectroelectrochemistry: Part I. Heterocyclic, aromatic, and aliphatic amines adsorbed on the anodized silver electrode. *J. Electroanal. Chem. Interfacial Electrochem.* 84:1–20
14. Albrecht MG, Creighton JA. 1977. Anomalously intense Raman spectra of pyridine at a silver electrode. *J. Am. Chem. Soc.* 99:5215–17

15. Le Ru EC, Etchegoin PG. 2008. *Principles of Surface-Enhanced Raman Spectroscopy and Related Plasmonic Effects*. Amsterdam: Elsevier
16. Langer J, de Aberasturi DJ, Aizpurua J, Alvarez-Puebla RA, Auguié B, et al. 2020. Present and future of surface-enhanced Raman scattering. *ACS Nano* 14:28–117
17. Wang X, Huang S-C, Hu S, Yan S, Ren B. 2020. Fundamental understanding and applications of plasmon-enhanced Raman spectroscopy. *Nat. Rev. Phys.* 2:253–71
18. Cortés E, Etchegoin PG, Le Ru EC, Fainstein A, Vela ME, Salvarezza RC. 2010. Monitoring the electrochemistry of single molecules by surface-enhanced Raman spectroscopy. *J. Am. Chem. Soc.* 132:18034–37
19. dos Santos DP, Andrade GFS, Temperini MLA, Brolo AG. 2009. Electrochemical control of the time-dependent intensity fluctuations in surface-enhanced Raman scattering (SERS). *J. Phys. Chem. C* 113:17737–44
20. Li J-F, Huang Y-F, Ding Y, Yang Z-L, Li S-B, et al. 2010. Shell-isolated nanoparticle-enhanced Raman spectroscopy. *Nature* 464:392–95
21. Li J-F, Zhang Y-J, Ding S-Y, Panneerselvam R, Tian Z-Q. 2017. Core–shell nanoparticle-enhanced Raman spectroscopy. *Chem. Rev.* 117:5002–69
22. Dong J-C, Zhang X-G, Briega-Martos V, Jin X, Yang J, et al. 2019. In situ Raman spectroscopic evidence for oxygen reduction reaction intermediates at platinum single-crystal surfaces. *Nat. Energy* 4:60–67
23. Li C-Y, Le J-B, Wang Y-H, Chen S, Yang Z-L, et al. 2019. In situ probing electrified interfacial water structures at atomically flat surfaces. *Nat. Mater.* 18:697–701
24. Ji Y, Dong J-C, Kumar VV, Li J-F, Tian Z-Q. 2017. Probing electrochemical interfaces using shell-isolated nanoparticles-enhanced Raman spectroscopy. *Curr. Opin. Electrochem.* 1:16–21
25. Sonnenfeld R, Schardt BC. 1986. Tunneling microscopy in an electrochemical cell: images of Ag plating. *Appl. Phys. Lett.* 49:1172–74
26. Robinson RS. 1988. Real-time scanning tunnelling microscopy of surfaces under active electrochemical control. *J. Microsc.* 152:541–46
27. Itaya K, Tomita E. 1988. Scanning tunneling microscope for electrochemistry - a new concept for the in situ scanning tunneling microscope in electrolyte solutions. *Surf. Sci.* 201:L507–12
28. Manne S, Massie J, Elings VB, Hansma PK, Gewirth AA. 1991. Electrochemistry on a gold surface observed with the atomic force microscope. *J. Vac. Sci. Technol. B* 9:950–54
29. Bard AJ, Fan F-RF, Kwak J, Lev O. 1989. Scanning electrochemical microscopy. Introduction and principles. *Anal. Chem.* 61:132–38
30. Hüsser OE, Craston DH, Bard AJ. 1989. Scanning electrochemical microscopy: high-resolution deposition and etching of metals. *J. Electrochem. Soc.* 136:3222–29
31. Bard AJ, Fan F-RF, Pierce DT, Unwin PR, Wipf DO, Zhou F. 1991. Chemical imaging of surfaces with the scanning electrochemical microscope. *Science* 254:68–74
32. Amemiya S, Bard AJ, Fan F-RF, Mirkin MV, Unwin PR. 2008. Scanning electrochemical microscopy. *Annu. Rev. Anal. Chem.* 1:95–131
33. Tian ZQ, Li WH, Ren B, Mao BW, Chen JG, et al. 1996. Simultaneous STM and Raman measurements on electrochemical interfaces. *J. Electroanal. Chem.* 401:247–51
34. Stöckle RM, Suh YD, Deckert V, Zenobi R. 2000. Nanoscale chemical analysis by tip-enhanced Raman spectroscopy. *Chem. Phys. Lett.* 318:131–36
35. Anderson MS. 2000. Locally enhanced Raman spectroscopy with an atomic force microscope. *Appl. Phys. Lett.* 76:3130–32
36. Hayazawa N, Inouye Y, Sekkat Z, Kawata S. 2000. Metallized tip amplification of near-field Raman scattering. *Opt. Commun.* 183:333–36
37. Pettinger B, Picardi G, Schuster R, Ertl G. 2000. Surface enhanced Raman spectroscopy: towards single molecule spectroscopy. *Electrochemistry* 68:942–49
38. Tian ZQ, Ren B. 2003. Raman spectroscopy of electrode surfaces. In *Encyclopedia of Electrochemistry*, Vol. 3, ed. AJ Bard, M Stratmann, PR Unwin, pp. 576–659. Weinheim, Ger.: Wiley-VCH
39. Zeng Z-C, Huang S-C, Wu D-Y, Meng L-Y, Li M-H, et al. 2015. Electrochemical tip-enhanced Raman spectroscopy. *J. Am. Chem. Soc.* 137:11928–31
40. Kurouski D, Mattei M, Van Duyne RP. 2015. Probing redox reactions at the nanoscale with electrochemical tip-enhanced Raman spectroscopy. *Nano Lett.* 15:7956–62

41. Yokota Y, Hayazawa N, Yang B, Kazuma E, Catalan FCI, Kim Y. 2019. Systematic assessment of benzenethiol self-assembled monolayers on Au(111) as a standard sample for electrochemical tip-enhanced Raman spectroscopy. *J. Phys. Chem. C* 123:2953–63
42. Martín Sabanés N, Driessen LMA, Domke KF. 2016. Versatile side-illumination geometry for tip-enhanced Raman spectroscopy at solid/liquid interfaces. *Anal. Chem.* 88:7108–14
43. Chen X, Goubert G, Jiang S, Van Duyne RP. 2018. Electrochemical STM tip-enhanced Raman spectroscopy study of electron transfer reactions of covalently tethered chromophores on Au(111). *J. Phys. Chem. C* 122:11586–90
44. Gjonaj B, Johnson P, Bonn M, Domke KF. 2012. Index mismatch aberration correction over long working distances using spatial light modulation. *Appl. Opt.* 51:8034–40
45. Huang S-C, Ye J-Z, Shen X-R, Zhao Q-Q, Zeng Z-C, et al. 2019. Electrochemical tip-enhanced Raman spectroscopy with improved sensitivity enabled by a water immersion objective. *Anal. Chem.* 91:11092–97
46. Zeng Z-C, Hu S, Huang S-C, Zhang Y-J, Zhao W-X, et al. 2016. Novel electrochemical Raman spectroscopy enabled by water immersion objective. *Anal. Chem.* 88:9381–85
47. Touzalin T, Joiret S, Lucas IT, Maisonhaute E. 2019. Electrochemical tip-enhanced Raman spectroscopy imaging with 8 nm lateral resolution. *Electrochem. Commun.* 108:106557
48. Bao Y-F, Cao M-F, Wu S-S, Huang T-X, Zeng Z-C, et al. 2020. Atomic force microscopy based top-illumination electrochemical tip-enhanced Raman spectroscopy. *Anal. Chem.* 92:12548–55
49. Ren B, Picardi G, Pettinger B. 2004. Preparation of gold tips suitable for tip-enhanced Raman spectroscopy and light emission by electrochemical etching. *Rev. Sci. Instrum.* 75:837–41
50. Yang B, Kazuma E, Yokota Y, Kim Y. 2018. Fabrication of sharp gold tips by three-electrode electrochemical etching with high controllability and reproducibility. *J. Phys. Chem. C* 122:16950–55
51. Zhang W, Yeo BS, Schmid T, Zenobi R. 2007. Single molecule tip-enhanced Raman spectroscopy with silver tips. *J. Phys. Chem. C* 111:1733–38
52. Yeo B-S, Zhang W, Vannier C, Zenobi R. 2006. Enhancement of Raman signals with silver-coated tips. *Appl. Spectrosc.* 60:1142–47
53. Barrios CA, Malkovskiy AV, Kisliuk AM, Sokolov AP, Foster MD. 2009. Highly stable, protected plasmonic nanostructures for tip enhanced Raman spectroscopy. *J. Phys. Chem. C* 113:8158–61
54. Peng L, Lee H, Teizer W, Liang H. 2009. Nanowear of gold and silver against silicon. *Wear* 267:1177–80
55. Yang L-K, Huang T-X, Zeng Z-C, Li M-H, Wang X, et al. 2015. Rational fabrication of a gold-coated AFM TERS tip by pulsed electrodeposition. *Nanoscale* 7:18225–31
56. Huang T-X, Li C-W, Yang L-K, Zhu J-F, Yao X, et al. 2018. Rational fabrication of silver-coated AFM TERS tips with a high enhancement and long lifetime. *Nanoscale* 10:4398–405
57. Saito Y, Murakami T, Inouye Y, Kawata S. 2005. Fabrication of silver probes for localized plasmon excitation in near-field Raman spectroscopy. *Chem. Lett.* 34:920–21
58. Brejna PR, Griffiths PR. 2010. Electroless deposition of silver onto silicon as a method of preparation of reproducible surface-enhanced Raman spectroscopy substrates and tip-enhanced Raman spectroscopy tips. *Appl. Spectrosc.* 64:493–99
59. Huang T-X, Huang S-C, Li M-H, Zeng Z-C, Wang X, Ren B. 2015. Tip-enhanced Raman spectroscopy: tip-related issues. *Anal. Bioanal. Chem.* 407:8177–95
60. Wang X, Huang S-C, Huang T-X, Su H-S, Zhong J-H, et al. 2017. Tip-enhanced Raman spectroscopy for surfaces and interfaces. *Chem. Soc. Rev.* 46:4020–41
61. Chen X, Brasiliense V, Van Duyne RP. 2018. Operando observation of molecular-scale manipulation using electrochemical tip-enhanced Raman spectroscopy. *J. Phys. Chem. C* 122:24329–33
62. Goubert G, Chen X, Jiang S, Van Duyne RP. 2018. *In situ* electrochemical tip-enhanced Raman spectroscopy with a chemically modified tip. *J. Phys. Chem. Lett.* 9:3825–28
63. Chen Z, Jiang S, Kang G, Nguyen D, Schatz GC, Van Duyne RP. 2019. Operando characterization of iron phthalocyanine deactivation during oxygen reduction reaction using electrochemical tip-enhanced Raman spectroscopy. *J. Am. Chem. Soc.* 141:15684–92
64. Jiang S, Chen Z, Chen X, Nguyen D, Mattei M, et al. 2019. Investigation of cobalt phthalocyanine at the solid/liquid interface by electrochemical tip-enhanced Raman spectroscopy. *J. Phys. Chem. C* 123:9852–59

65. Schmid T, Yeo B-S, Leong G, Stadler J, Zenobi R. 2009. Performing tip-enhanced Raman spectroscopy in liquids. *J. Raman Spectrosc.* 40:1392–99
66. Kumar N, Su W, Veselý M, Weckhuysen BM, Pollard AJ, Wain AJ. 2018. Nanoscale chemical imaging of solid–liquid interfaces using tip-enhanced Raman spectroscopy. *Nanoscale* 10:1815–24
67. Pourbaix M. 1974. *Atlas of Electrochemical Equilibria in Aqueous Solutions*. Houston, TX: Natl. Assoc. Corros. Eng.
68. Kumar N, Wondergem CS, Wain AJ, Weckhuysen BM. 2019. In situ nanoscale investigation of catalytic reactions in the liquid phase using zirconia-protected tip-enhanced Raman spectroscopy probes. *J. Phys. Chem. Lett.* 10:1669–75
69. Huang Y-P, Huang S-C, Wang X-J, Bodappa N, Li C-Y, et al. 2018. Shell-isolated tip-enhanced Raman and fluorescence spectroscopy. *Angew. Chem. Int. Ed.* 57:7523–27
70. Kelly KL, Coronado E, Zhao LL, Schatz GC. 2003. The optical properties of metal nanoparticles: the influence of size, shape, and dielectric environment. *J. Phys. Chem. B* 107:668–77
71. McFarland AD, Van Duyne RP. 2003. Single silver nanoparticles as real-time optical sensors with zeptomole sensitivity. *Nano Lett.* 3:1057–62
72. Mock JJ, Smith DR, Schultz S. 2003. Local refractive index dependence of plasmon resonance spectra from individual nanoparticles. *Nano Lett.* 3:485–91
73. Miller MM, Lazarides AA. 2005. Sensitivity of metal nanoparticle surface plasmon resonance to the dielectric environment. *J. Phys. Chem. B* 109:21556–65
74. Cui X, Zhang W, Yeo B-S, Zenobi R, Hafner C, Erni D. 2007. Tuning the resonance frequency of Ag-coated dielectric tips. *Opt. Express* 15:8309–16
75. Taguchi A, Hayazawa N, Saito Y, Ishitobi H, Tarun A, Kawata S. 2009. Controlling the plasmon resonance wavelength in metal-coated probe using refractive index modification. *Opt. Express* 17:6509–18
76. Maouli I, Taguchi A, Saito Y, Kawata S, Verma P. 2015. Optical antennas for tunable enhancement in tip-enhanced Raman spectroscopy imaging. *Appl. Phys. Express* 8:032401
77. Zou Y, Steinvurzel P, Yang T, Crozier KB. 2009. Surface plasmon resonances of optical antenna atomic force microscope tips. *Appl. Phys. Lett.* 94:171107
78. Vasconcelos TL, Archanjo BS, Oliveira BS, Valaski R, Cordeiro RC, et al. 2018. Plasmon-tunable tip pyramids: monopole nanoantennas for near-field scanning optical microscopy. *Adv. Opt. Mater.* 6:1800528
79. Vasconcelos TL, Archanjo BS, Fragneaud B, Oliveira BS, Riikonen J, et al. 2015. Tuning localized surface plasmon resonance in scanning near-field optical microscopy probes. *ACS Nano* 9:6297–304
80. Martín Sabanés N, Ohto T, Andrienko D, Nagata Y, Domke KF. 2017. Electrochemical TERS elucidates potential-induced molecular reorientation of adenine/Au(111). *Angew. Chem. Int. Ed.* 56:9796–801
81. Mattei M, Kang G, Goubert G, Chulhai DV, Schatz GC, et al. 2017. Tip-enhanced Raman voltammetry: coverage dependence and quantitative modeling. *Nano Lett.* 17:590–96
82. Zaleski S, Wilson AJ, Mattei M, Chen X, Goubert G, et al. 2016. Investigating nanoscale electrochemistry with surface- and tip-enhanced Raman spectroscopy. *Acc. Chem. Res.* 49:2023–30
83. Kang G, Yang M, Mattei MS, Schatz GC, Van Duyne RP. 2019. *In situ* nanoscale redox mapping using tip-enhanced Raman spectroscopy. *Nano Lett.* 19:2106–13
84. Pfisterer JHK, Baghernejad M, Giuzio G, Domke KF. 2019. Reactivity mapping of nanoscale defect chemistry under electrochemical reaction conditions. *Nat. Commun.* 10:5702
85. Huang S-C, Wang X, Zhao Q-Q, Zhu J-F, Li C-W, et al. 2020. Probing nanoscale spatial distribution of plasmonically excited hot carriers. *Nat. Commun.* 11:4211
86. Maouli I, Taguchi A, Saito Y, Kawata S, Verma P. 2015. Optical antennas for tunable enhancement in tip-enhanced Raman spectroscopy imaging. *Appl. Phys. Express* 8:032401
87. Hartschuh A, Sánchez EJ, Xie XS, Novotny L. 2003. High-resolution near-field Raman microscopy of single-walled carbon nanotubes. *Phys. Rev. Lett.* 90:095503
88. Tallarida N, Lee J, Apkarian VA. 2017. Tip-enhanced Raman spectromicroscopy on the angstrom scale: bare and CO-terminated Ag tips. *ACS Nano* 11:11393–401
89. Zhang C, Gao B, Chen LG, Meng QS, Yang H, et al. 2011. Fabrication of silver tips for scanning tunneling microscope induced luminescence. *Rev. Sci. Instrum.* 82:083101
90. Wickramasinghe HK, Chaigneau M, Yasukuni R, Picardi G, Ossikovski R. 2014. Billion-fold increase in tip-enhanced Raman signal. *ACS Nano* 8:3421–26

91. Pienpinijtham P, Vantasin S, Kitahama Y, Ekgasit S, Ozaki Y. 2016. Nanoscale pH profile at a solution/solid interface by chemically modified tip-enhanced Raman scattering. *J. Phys. Chem. C* 120:14663–68
92. Zong C, Chen C-J, Zhang M, Wu D-Y, Ren B. 2015. Transient electrochemical surface-enhanced Raman spectroscopy: a millisecond time-resolved study of an electrochemical redox process. *J. Am. Chem. Soc.* 137:11768–74
93. Nanda J, Yang G, Hou T, Voylov DN, Li X, et al. 2019. Unraveling the nanoscale heterogeneity of solid electrolyte interphase using tip-enhanced Raman spectroscopy. *Joule* 3:2001–19